



# Spectroscopy of the spin waves of a synthetic antiferromagnet grown on a piezoelectric substrate

G. Y. Thiancourt , S. M. Ngom, N. Bardou, and T. Devolder  <sup>a)</sup>

*Université Paris-Saclay, CNRS, Centre de Nanosciences et de Nanotechnologies, 91120, Palaiseau, France*

(Dated: 28 November 2024)

Efficient coupling between magnons and phonons requires material platforms that contain magnetic multilayers with versatile high-frequency properties grown on piezoelectric substrates with large electromechanical coupling coefficients. One of these systems is the CoFeB/Ru/CoFeB Synthetic antiferromagnet grown on Lithium Niobate substrate. We investigate its microwave magnetic properties using a combination of ferromagnetic resonance and propagating spin wave spectroscopy, from which we extract the dispersion relation of the acoustic branch of spin waves. The frequency and the linewidth of this spin wave resonance, its field dependence and its dispersion relation indicate that the magnetic properties are as good as when grown on standard non-piezoelectric substrates, as well as being in line with theory. This new material platform opens opportunities to extend microwave acousto-magnonics beyond the use of single layer magnets.

## I. INTRODUCTION

Devices exploiting surface acoustic waves (SAWs) play a significant role in numerous modern technological applications, ranging from wireless communications<sup>1</sup> to medicine<sup>2</sup>, sensors<sup>3</sup>, and RF signal processing in telecommunications. However, they have certain limitations, such as a reciprocal propagation and the near-absence of tunability. Circumventing these limitations may be possible by coupling SAWs with magnons<sup>4–11</sup> since the latter feature tunability and non-reciprocity. In particular, the spin waves (SWs) within magnetic bilayers have attracted interest<sup>12</sup> because of their convenient high frequency SWs with long propagation lengths. Ensuring the high quality of both the magnetic thin film and the piezoelectric substrate is crucial to benefit from the SAW-SW coupling.

In this study, we investigate SWs within a synthetic antiferromagnet (SAF) grown on a piezoelectric lithium niobate substrate LiNbO<sub>3</sub>. The SAF consists of two magnetic layers of CoFeB, separated by a non-magnetic spacer layer mediating antiferromagnetic coupling. The SAF exhibits two eigenmodes: the optical mode and the acoustic mode, characterized by out-of-phase and in-phase precession of the magnetizations, respectively<sup>13–18</sup>. It is known that the SW properties are very sensitive to the material structure, the roughness and the interdiffusion inside the stack<sup>19</sup>. Here we measure the properties of acoustic SWs using inductive techniques and demonstrate that it is possible to grow high-quality SAFs on high performing LiNbO<sub>3</sub> piezoelectric substrates.

## II. MATERIALS AND DEVICES

We use a SAF of composition LiNbO<sub>3</sub> (Y-cut substrate)/Ta /Co<sub>40</sub>Fe<sub>40</sub>B<sub>20</sub>( $t_{\text{mag}} = 17$  nm) /Ru(0.7nm) /Co<sub>40</sub>Fe<sub>40</sub>B<sub>20</sub>( $t_{\text{mag}}$ ) /Ru /Ta(cap) [Fig. 1.(a)]. The CoFeB has a magnetization  $\mu_0 M_s = 1.7$  T and an inter-layer exchange field  $\mu_0 H_j \approx 100$  mT. We pattern<sup>18</sup> the SAF into stripes of width  $w_{\text{mag}} = 20$   $\mu\text{m}$  and much longer length. We cover the sample with Si<sub>3</sub>N<sub>4</sub> and fabricate two micrometer-sized single wire antennas of widths  $w_{\text{ant}}$  and variable center-to-center distances  $r$  from 3.4 to 6  $\mu\text{m}$  [Fig. 1(c)]. This device will be used to perform propagating spin waves spectroscopy (PSWS) and compare the material quality to existing benchmarks. The analysis of PSWS data will require the knowledge of the resonant frequencies  $\omega(k=0)$  of uniform SWs, for which we fabricate an additional device to perform VNA-FMR<sup>20</sup>. To ensure comparability, the VNA-FMR device is built on the same chip as the PSWS device. It consists of an array of circular 4  $\mu\text{m}$  dots<sup>21</sup> inductively coupled to a much wider coplanar waveguide [Fig. 1(b)], which excites the uniform SW modes. The linewidth and the resonant frequencies of the uniform acoustic and optical spin wave modes shall provide the value of  $H_j$  and of the damping parameter  $\alpha$ .

## III. FERROMAGNETIC RESONANCE OF THE ACOUSTIC SPIN WAVES

Fig. 2 summarizes the results obtained by VNA-FMR. The resonant frequency of the acoustic spin wave (pink curve) of the dots evolves quasi-linearly with the applied field. The resonance has the classical Lorentzian line shape (inset in Fig. 2), with a full width at half maximum that is almost independent of the field, being for instance 370 MHz for an applied field of  $\mu_0 H_x = 50$  mT leading to a resonant frequency of  $f_{\text{dots}}(k=0) = 6.49$  GHz. The analysis of the linewidth using ref. 22 yields a Gilbert damping of  $\alpha = \Delta\omega_0/(\gamma_0(M_s + H_j)) = 0.006 \pm 0.001$ ,

<sup>a)</sup>Electronic mail: thibaut.devolder@cnrs.fr

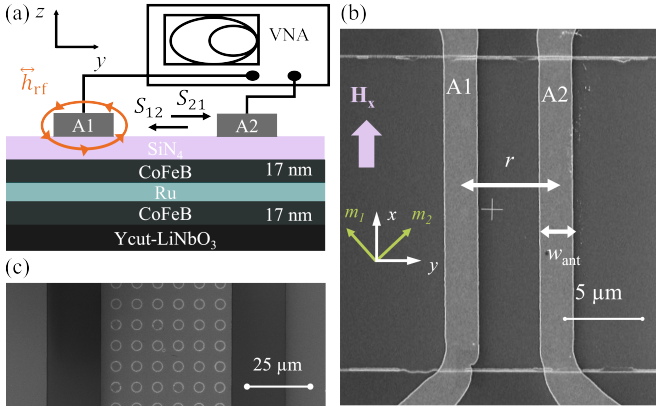


FIG. 1. (a) Sketch of the setup of propagating spin wave spectroscopy (PSWS). (b) Scanning electron microscopy image of a PSWS device. Light gray: single-wire antennas. Medium gray: Synthetic antiferromagnet conduit. (c) of array of SAF dots covered by a coplanar waveguide meant to measure VNA-FMR.

where  $\gamma_0$  is the gyromagnetic ratio.

Because of shape anisotropy, the uniform resonance of the dots differs from the uniform resonance of the stripe on which PSWS will be performed. Let us model this difference using the demagnetizing factors of our geometries  $\vec{N} = \{N_x, N_y, N_z\}$ . Using Eq. 11 of 23, the demagnetizing factors of each layer of the dot are  $\vec{N}_{\text{dot}} = \{0.01, 0.01, 0.98\}$ . Using 24, the demagnetizing tensor of each layer of the stripe is  $\vec{N}_{\text{stripe}} = \{0.004, 0.001, 0.995\}$ . Since  $N_y \leq N_x \ll N_z$ ,  $\pm y$  is the easy axis and we can define a shape anisotropy field as  $H_k = (N_x - N_y)M_s > 0$ . We also define the saturation fields  $H_{\text{sat},x} = H_j + H_k$  and  $H_{\text{sat},y} = H_j - H_k$  for saturation by fields in either the  $x$  or the  $y$  direction.

For a field of magnitude  $H_k < H_x < H_{\text{sat}}$  applied in the  $x$  direction, the SAF stripe is in a scissors state with the layers' magnetizations being:

$$\begin{cases} m_{x1} = m_{x2} = \frac{H_x}{H_{\text{sat},x}} \\ m_{y1} = -m_{y2} \\ m_{z1} = m_{z2} = 0 \end{cases} \quad (1)$$

Linearization of the equations of motions can be used to derive the frequency of the acoustic spin wave:

$$\omega_{\text{acou}} = \gamma_0 H_x \sqrt{H_j + (N_z - N_y)M_s} \times \sqrt{\frac{H_{\text{sat},x}}{H_{\text{sat},y}^2} - \frac{H_k}{H_x^2}} \quad (2)$$

We have deduced  $f_{\text{acou}}^{\text{stripe}}(H_x)$  from  $f_{\text{acou}}^{\text{dots}}(H_x)$ ,  $\vec{N}_{\text{stripe}}$ ,  $\vec{N}_{\text{dot}}$  and Eq. 2. The expected uniform resonance frequencies of the magnetic stripes for an applied field  $\mu_0 H_x = 50$  mT is for instance  $f_{\text{acou}}^{\text{stripe}}(H_x) = 6.44$  GHz. The resonance frequencies and their linewidth are very

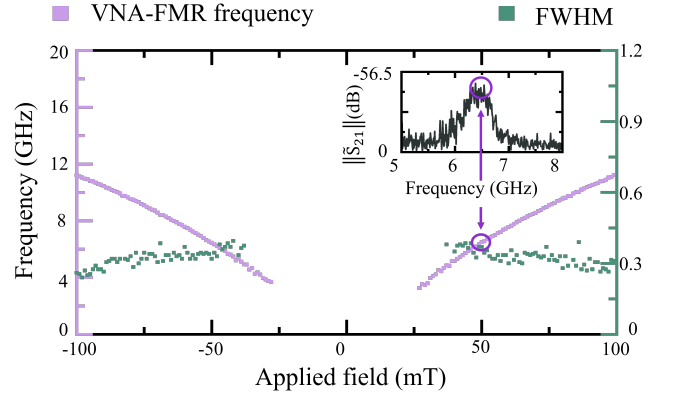


FIG. 2. VNA-FMR measurements of the uniform acoustic spin wave resonance in the array of  $4 \mu\text{m}$  dots. Left scale: Resonant frequencies as function of the applied field. The data correspond to the frequencies at which  $\|\hat{S}_{21}\|$  is maximal (inset). Right scale: Full widths at half maximum of these resonances.

similar to that of samples grown on non-piezoelectric substrates<sup>25,26</sup>. This is a first indicating that high quality SAF can be grown also on piezoelectric substrates. Let us determine the spin wave dispersion relation and its field dependence to assess this statement in a more quantitative way.

#### IV. SPIN WAVE SPECTROSCOPY OF THE ACOUSTIC SPIN WAVES OF THE SYNTHETIC ANTIFERROMAGNETS

##### A. Propagating spin wave measurements and methods

To get the dispersion relations, we performed propagating spin wave spectroscopy. We use the standard method and connect the two antennas A1 and A2 to the two ports of a calibrated VNA to measure the forward  $\hat{S}_{21}$  and backward  $\hat{S}_{12}$  transmission parameters for various applied field [Fig. 1(a)]. The SWs of SAF in this field configuration are known (and were checked) to be frequency-reciprocal<sup>17</sup>. The data processing meant to maximize the signal-to-noise ratio is carried out following the time-gating and field-differentiation methods detailed in refs. 27 and 18.

Fig 3.(a) shows the impulse response  $s_{12}(t)$  for a SW propagation distance  $r = 4.2 \mu\text{m}$ . The wavepackets of the acoustic SWs reach the second antenna in a travel time of typically  $t_g \approx 1$  ns. This group delay is essentially independent of the applied fields for fields inducing a scissor state<sup>28</sup> [see the dashed line in Fig 3(a)]. This group delay yields a first estimate of the group velocity of  $v_g \approx r/t_g = 4.2 \text{ km.s}^{-1}$  and a first estimate of the attenuation length of  $L_{\text{att}} = \frac{2v_g}{\Delta\omega_0} = 3.6 \mu\text{m}$  of the propagating acoustic spin waves.

Fig 3(b) shows a representative processed transmis-

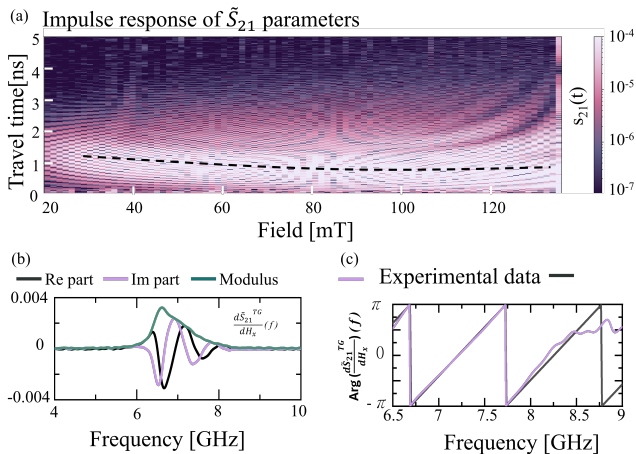


FIG. 3. Propagating Spin Wave Spectroscopy of the acoustic spin waves channeled in the SAF stripe. (a) Impulse response of the antenna-to-antenna forward transmission coefficient. The black line is a guide to the eye that tracks the time at which the signal of the acoustic SW wavepacket is maximum. (b) Field derivative of the forward transmission parameter  $\tilde{S}_{21}(f)$  for an applied field  $\mu_0 H_x = 50$  mT after time-gating. (c) Comparison of the experimental phase at  $\mu_0 H_x = 50$  mT with Eq. 5. Starting from the experimental estimates of Eq. 2, the parameters were fitted to be  $L_{\text{att}} = 3.6 \mu\text{m}$ ,  $r = 4.2 \mu\text{m}$ ,  $v_g = 4.4 \text{ km.s}^{-1}$  and  $f(k=0) = 6.43 \text{ GHz}$ .

sion spectrum around the frequency of the acoustic spin waves. The phase of the signal is reported in Fig 3(c). Transforming these phases into dispersion relations requires the modeling of the device's response.

## B. Model of $\tilde{S}_{21}$ for reciprocal spin waves

For reciprocal waves with a V-shaped dispersion relation, the contribution  $\tilde{S}_{21}^{yy}$  of the diagonal terms of the magnetic susceptibility to the forward transmission coefficient can be deduced from the sum of the experimental forward and reverse transmission coefficients (see the section IX.B of ref. 29):

$$\tilde{S}_{21}^{yy}(\omega, r, \nu) = \frac{1}{2} \left( S_{21}^{\text{exp}}(\omega) + S_{12}^{\text{exp}}(\omega) \right) \quad (3)$$

We consider in addition the limit of an ultra-thin antenna placed close to the magnetic film. Using the formalism of ref. 29, we can reformulate an expression of  $\tilde{S}_{21}(\omega)$  for reciprocal SWs with a V-shaped dispersion relation. Apart very near the uniform acoustic resonance, the scattering parameters can be expressed as<sup>29</sup>:

$$\tilde{S}_{21}^{yy}(k > \frac{\Delta\omega_0}{v_g}, r, \nu) = \sqrt{\frac{\pi}{2}} \mathcal{L}(k) \left( P_2(r - w_{\text{ant}}, k) + P_2(r + w_{\text{ant}}, k) - 2P_2(r, k) \right) \quad (4)$$

for  $k > \frac{\Delta\omega_0}{v_g}$ , with  $\mathcal{L}(k) \propto v_g^{-2} (k - i/L_{\text{att}})^{-2}$  a Lorentzian function centered at  $k = 0$  and of width

related to the inverse attenuation length<sup>30</sup>. The propagation term is expressed using the function  $P_2(x, k) = |L_{\text{att}}| e^{ikx} e^{-|L_{\text{att}} \frac{x}{L_{\text{att}}}|}$  that expresses the phase rotation and the decay of the wave upon its propagation.

Using Eq. 2 and 4 and taking into consideration that  $w_{\text{ant}} < r \ll L_{\text{att}}$ , we can state that for  $k > \frac{2}{L_{\text{att}}}$  the experimental data can be linked to the SW wavevector of the acoustic SW branch by:

$$\arg \left( \frac{\partial \tilde{S}_{21}^{yy}}{\partial H_x}(\omega) \right) = kr - \tan^{-1} \left( \frac{kL_{\text{att}}}{4} \right) + 2n\pi, \quad (5)$$

with  $n \in \mathbb{Z}$ . The value of  $n$  can be found from the frequency of the uniform mode ( $k = 0$ ) determined in section II. The equation 5 expresses that the phase of the field derivative of  $\tilde{S}_{21}^{yy}(\omega)$  parameter evolves linearly with the wavevector with a distance independent correction term. This correction term can be rewritten as  $\tan^{-1} \left( \frac{\omega - \omega_0}{2\Delta\omega_0} \right)$  to evidence that it tends towards  $\frac{\pi}{2}$  when working at frequencies  $\omega > \omega_0 + 2\Delta\omega_0$ . Fig. 3(c) shows the comparison of the experimental phase of the field derivative of  $\tilde{S}_{21}(f)$  with Eq. 5 for input values adjusted according to experimental measurements. The agreement is satisfactory and the dispersion relation can thus be deduced from a fit to Eq. 5.

## C. Dispersion relation of the acoustic spin waves

Fig. 4(a) gathers the dispersion relations of the acoustic SWs measured for applied field spanning from 30 mT up to 139 mT. This extends up to the maximum wavevector  $k_{\text{max}} \approx 3 \text{ rad}/\mu\text{m}$  that can be investigated with our antenna width. The  $k_y < 0$  part of the dispersion relations are constructed by symmetry.

For each applied field, the quasi-linear V-shape of the dispersion relation allows to define a characteristic group velocity. Fig. 4(b) reports the group velocity of SW deduced from linear fits done in the 0.7 to 1.3  $\text{rad}/\mu\text{m}$  interval of wavevector. For  $\mu_0 H_x = 50$  mT the group velocity is  $4.422 \pm 0.062 \text{ km.s}^{-1}$ . It increases up to  $5.220 \pm 0.041 \text{ km.s}^{-1}$  for  $\mu_0 H_x = 85$  mT. The group velocities deduced from samples with different propagation distances match together within a standard deviation of typically 200 m/s [inset of Fig. 4(b)]. This consistency among different devices is indicative of a good homogeneity of the magnetic properties despite their growth on non-standard substrates.

The group velocity is found to increase with the applied field until it saturates and decreases slightly for  $\mu_0 H_x > 100$  mT. This behavior is in semi-quantitative agreement with the predictions for a 2-macrospin SAF<sup>17</sup>, for which when  $\vec{H}_x \perp \vec{k}_y$ , the group velocity is expected to be  $\frac{1}{2}\gamma_0 M_s t \frac{H_x}{H_j} \frac{M_s}{\sqrt{H_j(H_j + M_s)}} \text{sgn}(k_y)$  for  $H_x < H_j$  (corresponding to the scissors state), and then to be slightly decreasing following  $\frac{1}{2}\gamma_0 M_s t \frac{M_s}{\sqrt{H_x(H_x + M_s)}} \text{sgn}(k_y)$

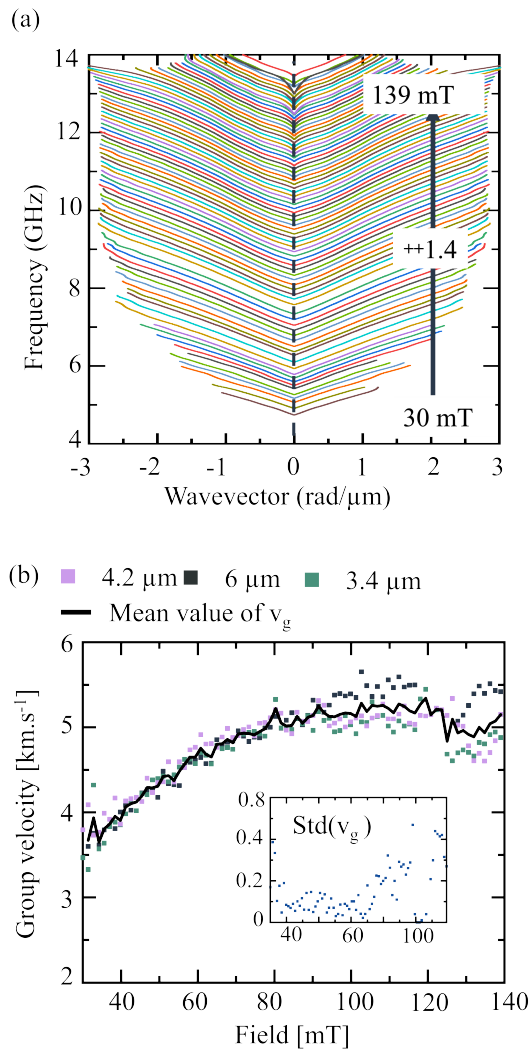


FIG. 4. (a) Dispersion relation of the acoustic spin waves for  $\vec{H}_x \perp \vec{k}$  obtained for a Propagating spin wave spectroscopy device with antenna width  $w_{\text{ant}} = 2 \mu\text{m}$  and antenna to antenna distance  $r = 4.2 \mu\text{m}$ . (b) Group velocities obtained for  $k=1 \text{ rad}/\mu\text{m}$  and  $r = 4.2 \mu\text{m}$  (violet),  $r = 6 \mu\text{m}$  (black) and  $r = 3.4 \mu\text{m}$  (green). Inset: standard deviation among these three measurements.

for larger fields (corresponding to the saturated parallel state). This is an additional indication of proper synthetic antiferromagnetic behavior.

## V. SUMMARY AND CONCLUDING REMARKS

In summary, we have measured several metrics representative of the dynamical properties of synthetic antiferromagnets grown on  $\text{LiNbO}_3$  substrates and patterned into magnonic devices. The measurements include the uniform resonance of the acoustic spin waves, the dispersion relation of these spin waves, and consequently their group velocities and attenuation lengths. These

metrics are indicative that the SAFs grown on  $\text{LiNbO}_3$  have very similar properties as the SAFs grown on standard non-piezoelectric substrates, for instance on silicon substrates<sup>17,25</sup>. The new material platform shall enable to efficiently couple the magnetic degrees of freedom to the elastic ones, for instance to confer non-reciprocity to surface acoustic wave delay lines<sup>31</sup>.

## ACKNOWLEDGMENTS

This work was supported by the French RENATECH network, by the French National Research Agency (ANR) as part of the ‘‘Investissements d’Avenir’’ and France 2030 programs. This includes the SPICY project of the Labex NanoSaclay: ANR-10-LABX-0035, the MAX-SAW project ANR-20-CE24-0025 and the PEPR SPIN projects ANR 22 EXSP 0008 and ANR 22 EXSP 0004. We acknowledge Aurélie Solognac for material growth and Loukas Kokkinos, Joo-Von Kim and Maryam Massouras for helpful comments.

## AUTHOR DECLARATIONS

### Conflict of Interest

The authors have no conflicts to disclose.

### Author Contributions

**G. Y. Thiancourt:** Data curation (lead); Formal analysis (lead); Writing– original draft (equal); Writing– review and editing (equal); Measurements (supporting); Investigation (equal). **S. M. Ngom:** Resources (equal); Investigation (equal); Measurements (equal). **N. Bardou:** Resources (equal). **T. Devolder:** Funding acquisition (lead); Investigation (equal); Measurements (equal); Writing– original draft (equal); Writing– review and editing (lead); Conceptualization (lead).

## DATA AVAILABILITY

The data that support the findings of this study are available within the article from the corresponding author upon reasonable request.

## REFERENCES

- <sup>1</sup>C. Campbell, ‘‘Surface acoustic wave devices for mobile and wireless communications, four-volume set,’’ (Academic Press, 1998).
- <sup>2</sup>K. Länge, B. E. Rapp, and M. Rapp, ‘‘Surface acoustic wave biosensors: a review,’’ *Analytical and bioanalytical chemistry* **391**, 1509–1519 (2008).

- <sup>3</sup>A. Pohl, “A review of wireless saw sensors,” *IEEE transactions on ultrasonics, ferroelectrics, and frequency control* **47**, 317–332 (2000).
- <sup>4</sup>C. Kittel, “Interaction of Spin Waves and Ultrasonic Waves in Ferromagnetic Crystals,” *Physical Review* **110**, 836–841 (1958).
- <sup>5</sup>L. Dreher, M. Weiler, M. Pernpeintner, H. Huebl, R. Gross, M. S. Brandt, and S. T. B. Goennenwein, “Surface acoustic wave driven ferromagnetic resonance in nickel thin films: Theory and experiment,” *Physical Review B* **86**, 134415 (2012).
- <sup>6</sup>M. Küß, S. Glamsch, Y. Kunz, A. Hörner, M. Weiler, and M. Albrecht, “Giant Surface Acoustic Wave Nonreciprocity with Low Magnetoacoustic Insertion Loss in CoFeB/Ru/CoFeB Synthetic Antiferromagnets,” *ACS Applied Electronic Materials* **5**, 5103–5110 (2023).
- <sup>7</sup>M. Küß, M. Heigl, L. Flacke, A. Hörner, M. Weiler, A. Wixforth, and M. Albrecht, “Nonreciprocal Magnetoacoustic Waves in Dipolar-Coupled Ferromagnetic Bilayers,” *Physical Review Applied* **15**, 034060 (2021).
- <sup>8</sup>M. Küß, M. Heigl, L. Flacke, A. Hefe, A. Hörner, M. Weiler, M. Albrecht, and A. Wixforth, “Symmetry of the Magnetoelastic Interaction of Rayleigh and Shear Horizontal Magnetoacoustic Waves in Nickel Thin Films on Li Ta O<sub>3</sub>,” *Physical Review Applied* **15**, 034046 (2021).
- <sup>9</sup>M. Huang, Y. Liu, W. Hu, Y. Wu, W. Wang, W. He, H. Zhang, and F. Bai, “Large nonreciprocity of shear-horizontal surface acoustic waves induced by a magnetoelastic bilayer,” *Physical Review Applied* **21**, 014035 (2024).
- <sup>10</sup>M. Xu, K. Yamamoto, J. Puebla, K. Baumgaertl, B. Rana, K. Miura, H. Takahashi, D. Grundler, S. Maekawa, and Y. Otani, “Nonreciprocal surface acoustic wave propagation via magnetorotation coupling,” *Science Advances* **6**, eabb1724 (2020).
- <sup>11</sup>K. Yamamoto, M. Xu, J. Puebla, Y. Otani, and S. Maekawa, “Interaction between surface acoustic waves and spin waves in a ferromagnetic thin film,” *Journal of Magnetism and Magnetic Materials* **545**, 168672 (2022).
- <sup>12</sup>J. H. Kwon, J. Yoon, P. Deorani, J. M. Lee, J. Sinha, K.-J. Lee, M. Hayashi, and H. Yang, “Giant nonreciprocal emission of spin waves in ta/py bilayers,” *Science Advances* **2**, e1501892 (2016).
- <sup>13</sup>R. L. Stamps, “Spin configurations and spin-wave excitations in exchange-coupled bilayers,” *Physical Review B* **49**, 339–347 (1994).
- <sup>14</sup>F. C. Nörtemann, R. L. Stamps, and R. E. Camley, “Microscopic calculation of spin waves in antiferromagnetically coupled multilayers: Nonreciprocity and finite-size effects,” *Physical Review B* **47**, 11910–11923 (1993).
- <sup>15</sup>M. Ishibashi, Y. Shiota, T. Li, S. Funada, T. Moriyama, and T. Ono, “Switchable giant nonreciprocal frequency shift of propagating spin waves in synthetic antiferromagnets,” *Science Advances* **6**, eaaz6931 (2020).
- <sup>16</sup>R. Gallardo, T. Schneider, A. Chaurasiya, A. Oelschlägel, S. Arekapudi, A. Roldán-Molina, R. Hübner, K. Lenz, A. Barmann, J. Fassbender, J. Lindner, O. Hellwig, and P. Landeros, “Reconfigurable Spin-Wave Nonreciprocity Induced by Dipolar Interaction in a Coupled Ferromagnetic Bilayer,” *Physical Review Applied* **12**, 034012 (2019).
- <sup>17</sup>F. Millo, J.-P. Adam, C. Chappert, J.-V. Kim, A. Mouhoub, A. Solignac, and T. Devolder, “Unidirectionality of spin waves in synthetic antiferromagnets,” *Physical Review Applied* **20**, 054051 (2023).
- <sup>18</sup>G. Thiancourt, S. Ngom, N. Bardou, and T. Devolder, “Unidirectional spin waves measured using propagating-spin-wave spectroscopy,” *Physical Review Applied* **22**, 034040 (2024).
- <sup>19</sup>A. Mouhoub, F. Millo, C. Chappert, J.-V. Kim, J. Létang, A. Solignac, and T. Devolder, “Exchange energies in CoFeB/Ru/CoFeB synthetic antiferromagnets,” *Physical Review Materials* **7**, 044404 (2023).
- <sup>20</sup>C. Bilzer, T. Devolder, P. Crozat, C. Chappert, S. Cardoso, and P. Freitas, “Vector network analyzer ferromagnetic resonance of thin films on coplanar waveguides: Comparison of different evaluation methods,” *Journal of applied physics* **101** (2007).
- <sup>21</sup>The geometry were chosen to reduce the effect of shape anisotropy.
- <sup>22</sup>T. Devolder, S.-M. Ngom, A. Mouhoub, J. Letang, J.-V. Kim, P. Crozat, J.-P. Adam, A. Solignac, and C. Chappert, “Measuring a population of spin waves from the electrical noise of an inductively coupled antenna,” *Physical Review B* **105**, 214404 (2022).
- <sup>23</sup>M. Beleggia, M. De Graef, and Y. Millev, “The equivalent ellipsoid of a magnetized body,” *Journal of Physics D: Applied Physics* **39**, 891 (2006).
- <sup>24</sup>A. Aharoni, “Demagnetizing factors for rectangular ferromagnetic prisms,” *Journal of applied physics* **83**, 3432–3434 (1998).
- <sup>25</sup>R. L. Seeger, F. Millo, A. Mouhoub, G. de Loubens, A. Solignac, and T. Devolder, “Inducing or suppressing the anisotropy in multilayers based on CoFeB,” *Physical Review Materials* **7**, 054409 (2023).
- <sup>26</sup>O. Wojewoda, J. Holobrádek, D. Pavelka, E. Pribytova, J. Krčma, J. Klíma, J. Michalička, T. Lednický, A. V. Chumak, and M. Urbánek, “Unidirectional propagation of zero-momentum magnons,” (2023), arXiv:2311.10044 [cond-mat].
- <sup>27</sup>T. Devolder, G. Talmelli, S. M. Ngom, F. Ciubotaru, C. Adelman, and C. Chappert, “Measuring the dispersion relations of spin wave bands using time-of-flight spectroscopy,” *Physical Review B* **103**, 214431 (2021).
- <sup>28</sup>For applied fields near and above saturation  $\mu_0 H_x \geq 100$  mT, the initially single wavepacket of the impulse response progressively splits into several separated wavepackets arriving at different  $t_g$ 's. This is indicative to the presence of several SW mode with different group velocities, most probably quantized in the width of the stripe<sup>22</sup>.
- <sup>29</sup>T. Devolder, “Propagating-spin-wave spectroscopy using inductive antennas: Conditions for unidirectional energy flow,” *Physical Review Applied* **20**, 054057 (2023).
- <sup>30</sup>We neglect any variation of the attenuation length with the wavevector.
- <sup>31</sup>R. Verba, V. Tiberkevich, and A. Slavin, “Wide-band nonreciprocity of surface acoustic waves induced by magnetoelastic coupling with a synthetic antiferromagnet,” *Physical Review Applied* **12**, 054061 (2019).